



## Configurational anisotropy in single-domain and pseudosingle-domain grains of magnetite

Wyn Williams,<sup>1</sup> Adrian R. Muxworthy,<sup>2</sup> and Greig A. Paterson<sup>3</sup>

Received 6 June 2006; revised 3 August 2006; accepted 17 August 2006; published 22 November 2006.

[1] In classical domain theory, single-domain (SD) grains change their magnetization by coherent rotation, where the energy barrier to domain reversal is provided by the magnetocrystalline anisotropy or by shape anisotropy for elongated grains. However, numerical micromagnetic models have shown that domain structure in SD grains is rarely perfectly uniform. For example, magnetite has significant “flowering” of its magnetization even in grains that approach the room temperature superparamagnetic (SP) size of  $\sim 30$  nm. The flowering deforms slightly to accommodate the grain shape and thereby produces anisotropy independent of magnetocrystalline effects but dependent on magnetization direction within the grain. This can be similar in magnitude to that of magnetocrystalline anisotropy, even for equidimensional grains (where distance from the centroid to the grain faces is equal). The interaction of the domain structure and grain geometry is termed configurational anisotropy and has been studied mainly in relation to man-made isotropic magnetic media but received little attention in rock magnetism. In this paper we examine configurational anisotropy in SD to pseudo-single-domain (PSD) grains of magnetite using a three-dimensional finite element/boundary integral (FEBI) micromagnetic model. Equidimensional grains of magnetite of three different shapes are considered: a cube, an octahedron, and a regular tetrahedron, and in each case the effects magnetocrystalline anisotropy were removed in order to isolate the configurational anisotropy. The numerical models predict that very large coercivities are possible even for SD equidimensional grains. For tetrahedral grains coercivities of  $\sim 120$  mT were obtained, which otherwise would require a grain elongation of  $\sim 1:1.75$ . Depending on the orientation of the principle crystalline axis to the grain shape, the configurational anisotropy may increase or decrease the overall energy barrier to domain reversal.

**Citation:** Williams, W., A. R. Muxworthy, and G. A. Paterson (2006), Configurational anisotropy in single-domain and pseudosingle-domain grains of magnetite, *J. Geophys. Res.*, *111*, B12S13, doi:10.1029/2006JB004556.

### 1. Introduction

[2] In paleomagnetism and environmental magnetism, magnetic hysteresis measurements are routinely made to determine the magnetic stability of a sample. Hysteresis knowledge can be used to quantify the reliability of a magnetic remanence signal carried by a rock, to estimate the grain size of the magnetic mineral within a sample or to help with mineral identification. Such information can be crucial in a variety of different studies, for example, paleoclimatic information is often revealed by subtle changes in grain size distribution, while the same grain size variations can complicate determination of the relative paleofield intensity from the same sediments.

[3] In rock magnetic studies of single-domain (SD) or pseudosingle-domain (PSD) magnetites, magnetic stability is usually ascribed to a variety of anisotropy sources, namely that of magnetocrystalline, shape or stress. The identification of the dominant contributor to the observed stability is usually done by comparison with standard measurements of hysteresis parameters, measured on laboratory manufactured samples of magnetite which are either acicular, or equidimensional octahedral in shape.

[4] The maximum coercivity of equidimensional magnetite grain is easily calculated for coherent rotation of uniform magnetization, as  $\sim 34$  mT. This value neglects the effects of thermal fluctuations, which we might expect to reduce coercivities by  $\sim 10$  mT [Dunlop and Özdemir, 1997]. Coercivities larger than this observed in magnetite are then attributed either to grain elongations or stress. However, this simple interpretation masks a much more complex process, which has long been acknowledged but rarely investigated in any detail. This is the interaction of inhomogeneous domains states with the grains shape, which is termed configurational anisotropy.

[5] Several previous studies have examined the effects of configurational anisotropy, but these have dealt mostly with

<sup>1</sup>School of Geosciences, University of Edinburgh, Edinburgh, UK.

<sup>2</sup>Department of Earth Science and Engineering, Imperial College, London, UK.

<sup>3</sup>National Oceanography Centre, University of Southampton, Southampton, UK.

two-dimensional structures, and usually formed from patterned thin films of isotropic magnetic materials [Koltsov *et al.*, 2000; Torres *et al.*, 2001; Vavassori *et al.*, 2005]. For naturally occurring magnetic materials, the influence of configurational anisotropy has received little attention. In this study we examine the possible contribution that configurational anisotropy can make to domains stability in SD and PSD magnetite grains by building a numerical micromagnetic model where the effects of other anisotropies, specifically that of shape and magnetocrystalline, can be removed.

## 2. Micromagnetic Method

[6] Micromagnetic models calculate stable magnetic structures by considering (usually) the balance between four forces. The first two of these are the externally applied magnetic field and the magnetocrystalline anisotropy, both of which are purely local in effect. The third force is due to the exchange interactions between neighboring atomic magnetic moments, and finally, the most CPU intensive calculation, is that of the long range and nonlinear internal demagnetizing field.

[7] Some care is needed in the choice of micromagnetic method employed. There are two main types of three-dimensional micromagnetic algorithms that have been developed in recent years. The finite difference (FD) method divides the geometry of a grain into a regular grid of cells, and the magnetization is resolved into magnetostatic “charges” on the surfaces of each cell [Williams and Dunlop, 1989; Williams and Wright, 1998]. This has considerable advantages in allowing computation of the demagnetizing fields in Fourier space; however, the imposition of a regular cell structure makes it difficult to model realistic grain shapes, although some progress in this has recently been made [Witt *et al.*, 2005].

[8] Accounting for the grain geometry is much more significant than mere shape aesthetics, since the present study examines the interaction between inhomogeneous domain structures and grain shape it is important account for the grain geometry as accurately as possible. We therefore use a hybrid finite element/boundary integral (FEBI) model similar to that of Fredkin and Koehler [1990] [see also Schrefl, 1999] where the geometry of the grain is filled with arbitrary shaped tetrahedral elements, and the magnetic forces are evaluated at the nodes located at the tetrahedral vertices. Although we can no longer calculate the demagnetizing fields in Fourier space, the FEBI method has the principle advantage over FD techniques in being able to accurately model the grain geometry.

[9] In our FEBI model, the grain geometries were meshed so as to ensure no tetrahedral element was bigger than the exchange length defined by  $\sqrt{A/K}$  [Rave *et al.*, 1998], where  $A$  is the exchange stiffness constant and  $K$  is the total magnetic anisotropy of any origin.

[10] The determination of equilibrium magnetic domain structures can be achieved most easily by searching for minimum energy structures, where the total free magnetic energy is expressed as

$$E_{\text{TOTAL}} = E_{\text{Crystalline Anisotropy}} + E_{\text{External Field}} + E_{\text{Exchange}} + E_{\text{Demagnetizing}}.$$

Minimum energy solvers, such as the conjugate gradient optimization methods that we have used previously [Wright *et al.*, 1997], are fast and efficient, but the magnetization structures are not constrained to follow a physically plausible path from the initial guess, and such algorithms can occasionally be prone to false convergence.

[11] More robust solutions can be obtained from following the dynamics of the magnetization when acted upon by a magnetic field. This is formulated in the Landau Lifshitz Gilbert (LLG) equation

$$\frac{d\mathbf{M}}{dt} = -\frac{\gamma}{1+\alpha^2}\mathbf{M} \times \mathbf{H}_{\text{eff}} + \frac{\alpha\gamma}{(1+\alpha^2)M_S}\mathbf{M} \times (\mathbf{M} \times \mathbf{H}_{\text{eff}})$$

Where  $\mathbf{M}$  is the unit vector along the magnetization direction,  $\gamma$  is the gyromagnetic ratio for an electron, and  $\alpha$  is a damping parameter.  $\mathbf{H}_{\text{eff}}$  is the effective field acting on the magnetization vector at each node of the finite element mesh, and this is made up from the four constituent fields similar to that for the calculation of the total magnetic energy and is related to the energy by

$$\mathbf{H}_{\text{eff}} = -\frac{1}{\mu_0} \frac{dE_{\text{TOTAL}}}{d\mathbf{M}}.$$

Although the LLG equation provides very robust solutions, it requires far more CPU time than those obtained from energy minimization alone. In our calculations, therefore, we used a combined algorithm, where we first performed a minimum energy search, and results of this were used as the initial guess to dynamic solution of the LLG equation.

[12] In order to examine configurational anisotropy we removed the magnetocrystalline contribution to the total magnetic energy and the effective field. Other than this modification the normal material parameters appropriate to magnetite at room temperature were used, namely the saturation magnetization ( $M_S = 4.8 \times 10^5 \text{ A m}^{-1}$ ), and exchange constant ( $A = 1.34 \times 10^{-11} \text{ J m}^{-1}$ ) [Heider and Williams, 1988; Pauthenet and Bochirol, 1951]. The value of the magnetocrystalline anisotropy used to calculate the exchange length was taken to be that of magnetite at room temperature ( $K = 1.24 \times 10^4 \text{ J m}^{-3}$ ), since it was expected that configurational anisotropy would be of a similar magnitude.

[13] Three simple grain shapes were chosen so as to represent equidimensional crystals with varying degrees of symmetry: (1) an octahedron and (2) a regular tetrahedron, both of which have equilateral triangular faces, and (3) a cube. For each of these shapes 10 different grain volumes were modeled, equivalent to the volume of a cube with an edge length between 24 nm and 200 nm.

## 3. Results

### 3.1. Zero-Field Domain Structures

[14] The zero-field magnetic structures that are expected to be nucleated in any SD or PSD grain are that of a flower-type state, vortex state or multiple-vortex state. In the grain size range that we consider here, only flower and single-vortex states are possible (Figure 1). These domain states deform to accommodate the geometry of the grain, and as a result there is an angular dependence of the magnetic energy of the domain state with respect to the grain geometry. This

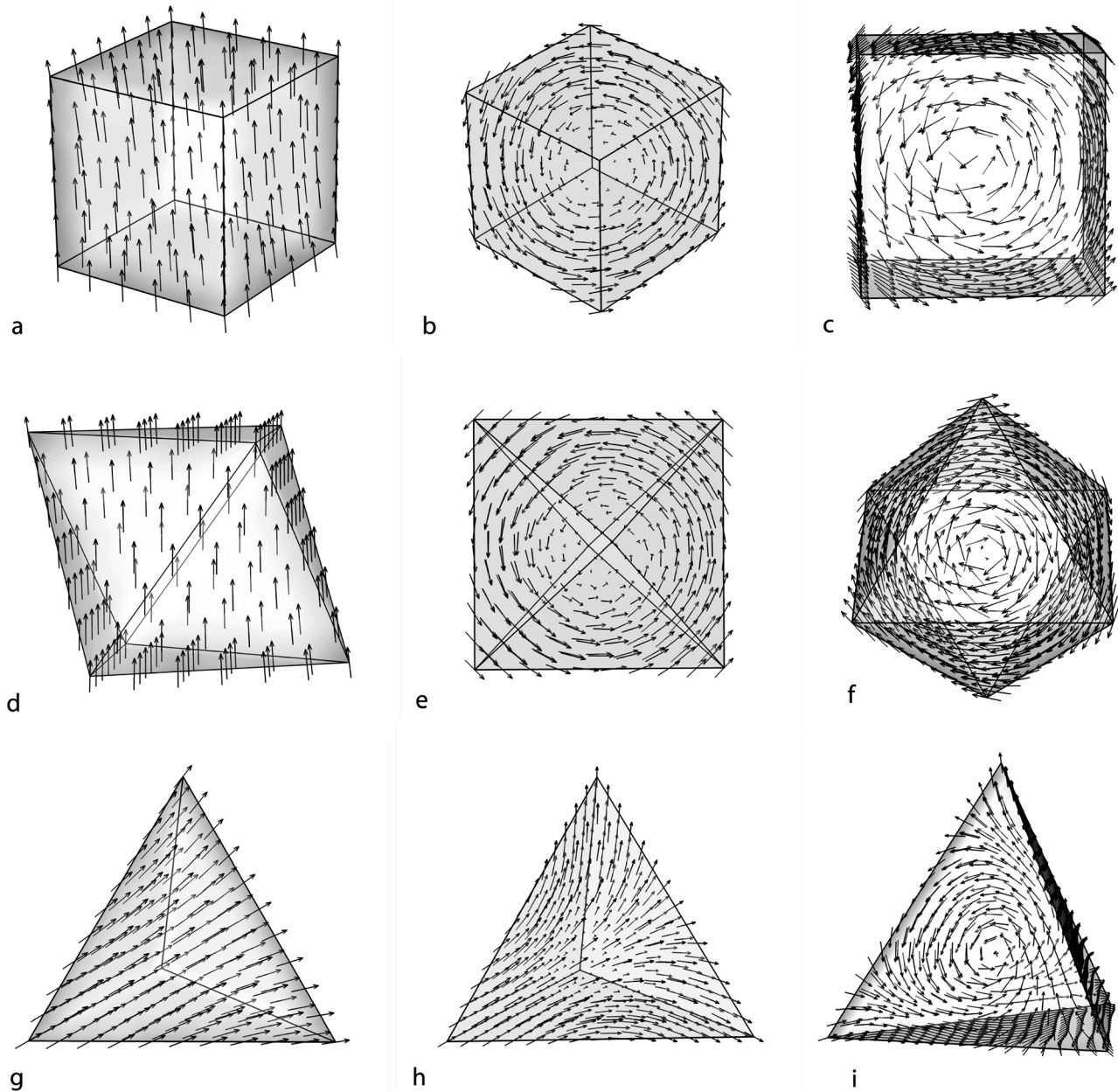


**Figure 1.** Zero-field magnetic domain structure in (a, b, and c) cubes, (d, e, and f) octahedral, and (g, h, and i) regular tetrahedra. The smallest grains corresponding to a grain geometry of  $(24 \text{ nm})^3$  (Figures 1a, 1d, and 1g) nucleate flower states oriented normal to a grain face in the cube (Figure 1a) and octahedron (Figure 1d), and points normal to a grain edge in the tetrahedron (Figure 1g). Above  $(70 \text{ nm})^3$  vortex states are nucleated in cubes (Figure 1b) and octahedra (Figure 1e), with the vortex core aligned along the grain diagonals. Flower states are still stable in tetrahedra due to the large amount of flowering that can be accommodated (Figure 1h). As the grain size increases further to  $(140 \text{ nm})^3$  the vortex cores are now aligned normal to a grain face (Figures 1c and 1f), and the vortex state is now also nucleated in the tetrahedra (Figure 1i).

angular dependence creates energy barriers to domain reversal, and can impart considerable magnetic stability.

[15] For equidimensional grains containing constrained, strictly uniform magnetization states, their energy is invariant to the direction of magnetization within them. This is easily shown to be true for the three geometries used in this investigation (see section 4.1), and demonstrates that any anisotropy exhibited in these grains must be due to the

interaction of nonuniform magnetizations with the grain geometry.

[16] In all three grain geometries, the smallest grains modeled, corresponding to a volume of  $(24 \text{ nm})^3$ , contain simple flower magnetic domain states (Figures 1a, 1d, and 1g). For the cube and octahedron, the average magnetization is aligned normal to a grain face, and for the tetrahedron, the magnetization is normal to a grain edge. Thus even in grains

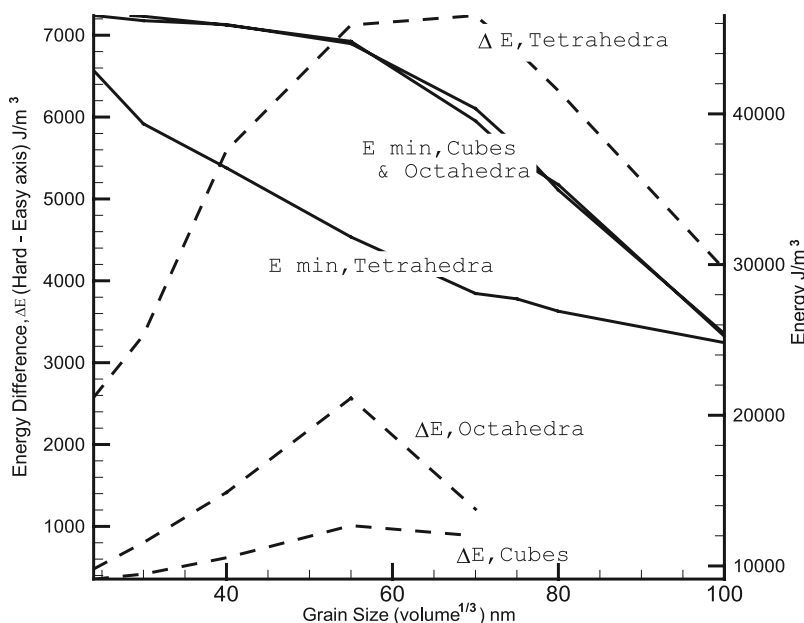


**Figure 2.** Energy of the zero-field domain states (solid lines), and the energy difference between the hard and easy direction of magnetization (dashed lines), for each of the three different grain geometries as a function of grain size.

smaller than the superparamagnetic grains size limit in magnetite of  $(\sim 30 \text{ nm})^3$ , configurational anisotropy plays an important role.

[17] As the grain size increases, vortex states are nucleated. In these magnetite grains, modeled with zero magneto-crystalline anisotropy, this occurs in cubic and octahedral grains above  $(70 \text{ nm})^3$  in volume. The tetrahedral grains of an equivalent volume are able to achieve much lower energy states than the other grain geometries (Figure 2), and so vortex minimum energy domain states do not appear until volumes greater than  $(140 \text{ nm})^3$ . The initial vortex states for the cubes and octahedra have the vortex cores aligned along a grain diagonal (Figures 1b and 1e), and as the grain size increases the core switches to be normal to a grain face (Figures 1c and 1f).

### 3.2. Hysteresis Parameters

[18] Each modeled grain was subject to a simulated quarter-loop hysteresis cycle. The field was applied antiparallel to the direction of the average magnetization at saturation remanence. That is, in an easy configurational anisotropy direction. For the cube and octahedron, this direction is normal to a grain face, and for the tetrahedron, it is normal to a grain edge. Thus the initial field value for the hysteresis simulations was 0 mT and equilibrium domain structures were then computed for field steps of between  $-2.0$  and  $-0.5$  mT, until a reverse field of  $-120$  mT is reached, or until the magnetization had attained saturation. At each field step, the initial guess of the magnetic structure for the energy minimization was the solution from integration of the LLG equation at the previous field step.

[19] The coercivity due to configurational anisotropy, and the saturation remanence, as a function of grain size are shown in Figure 3. Two peaks can be seen in the coercivity plot for the cubic and octahedral grains. The first peak

corresponds to the critical SD grain size, that is, the maximum grain size that can accommodate a flower state. For these geometries, as long as the grain remains in the flower state, its magnetic energy and energy barrier to domain rotation, increases with grain volume, resulting in higher coercivities. In this range the saturation remanence decreases as the amount of flowering increases.

[20] Above the critical SD grains size a vortex state is nucleated, with the vortex core aligned along a grain diagonal, as shown in Figures 1b and 1e. In any simple vortex state the major remanence is carried in the core itself, and since the core is not aligned in the direction of the field, the saturation remanence value drops sharply. Thus for the cubic grain, as the back field is increased along the  $[0 \bar{1} 0]$ , the core jumps from the  $[1 \bar{1} \bar{1}]$  to the  $[1 \bar{1} 1]$  direction. This coherent switching of the vortex core, requires less energy than domain reversal of the flower states, and so the coercivity is reduced. A similar process occurs in the octahedral grains of the same size, and for the tetrahedral grains at  $(140 \text{ nm})^3$ . For the tetrahedral grains, the vortex core is initially aligned parallel to a grain face, and the back field applied normal to this surface. Since this grain shape accommodates a much higher degree of flowering (termed a “Y” state in the case of triangular particles [Cowburn *et al.*, 1999; Koltsov *et al.*, 2000]) a vortex state is not achieved until  $(140 \text{ nm})^3$ . A peak in the coercivity is still observed at the same grain volume as that due to coherent rotation of flower states in the other geometries.

[21] At  $(75 \text{ nm})^3$  for the cubes, and  $(80 \text{ nm})^3$  for the octahedral grains, the remanence state switches from a vortex aligned with the grain vertices to parallel with a grain face. Since the vortex core is now aligned with the external field direction, the saturation remanence increases. Switching of the magnetization on application of the back field now occurs through reversal of the core magnetization

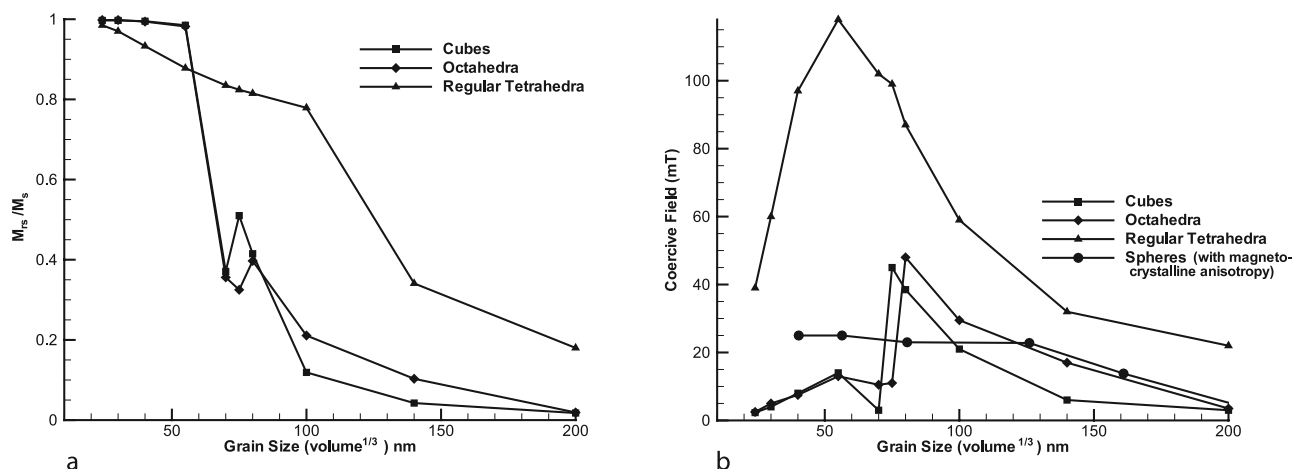


**Figure 3.** (a) Saturation remanence and (b) coercivity for magnetic fields applied along the easy configurational anisotropy axis and as a function of grain size for the three different grain geometries. The coercivity of spherical grains of magnetite (which includes magnetocrystalline anisotropy) is shown for comparison in Figure 3b.

itself, while the rest of the grain’s magnetization remains essentially unchanged.

### 3.3. Anisotropy Energy Surfaces

[22] Given that configurational anisotropy is an interaction between the domain state and the grains shape, it is expected that the symmetry of the anisotropy is the same as that of the grain geometry. The directions of the minimum and maximum magnetocrystalline anisotropy directions, and the energy barriers between the minimum energy states, can be determined by mapping out the anisotropy energy surface.

[23] Energy surfaces were produced in manner similar to that of *Enkin and Williams* [1994]. The magnetization of a relatively small fraction of the grain is constrained to lie in certain directions, and then an equilibrium solution is found subject to this constraint. Enkin and Williams examined only cubic shaped grains, and applied constraints to the magnetization on two opposing grain faces. This allowed the grain’s energy to be parameterized in terms of the angular deflection of the magnetization, within the plane, on these two opposing faces. In the present study we constrained the magnetization direction of 1% of the grain volume located at its centroid. The magnetization within the constrained volume was uniform, and the polar and azimuthal angles  $(\theta_i, \phi_i)$  were set at fixed values from  $0 \leq \theta_i \leq 180$ ,  $0 \leq \phi_i < 360$ , and the equilibrium domain structures determined. This method is able to provide an estimate of the configurational anisotropy energy surface for grains containing flower domains states only. For vortex states, the constraint of a uniformly magnetized region at the center of a grain will slightly distort the vortex geometry, and so the corresponding energy surface will also be distorted.

[24] We calculated the configurational anisotropy energy surfaces for grains volumes  $(24 \text{ nm})^3 < V < (55 \text{ nm})^3$ , for which flower states exist in all three grains geometries. The results are plotted in Figure 4, along with the energy surface due to the cubic magnetocrystalline of magnetite anisotropy alone. The cube’s configurational anisotropy (Figures 4a–4c) displays the same shape as that of metallic iron, i.e., cubic

anisotropy with a positive  $K_1$ , while octahedral display a configurational anisotropy (Figures 4d–4f), which displays the same symmetry as magnetite, i.e., cubic anisotropy with a negative  $K_1$  (Figure 4j). The configurational anisotropy for the tetrahedra (Figures 4g–4i) is similar to that of the cube, but is rotated by  $45^\circ$  from the horizontal. Increasing the volume of the grain, makes the configurational anisotropy less rounded in appearance.

## 4. Discussion

[25] The importance of configurational anisotropy can be easily appreciated by comparison with the well-understood sources of anisotropy, namely that due to (1) magnetocrystalline anisotropy and (2) grain elongation (commonly termed “shape” anisotropy).

### 4.1. Anisotropy Energy Surfaces

[26] The anisotropy energy surfaces (Figure 4), demonstrate that there are easy and hard directions of magnetization that relate directly to the way the domain structure interacts with the grain shape. In all the equidimensional geometries modeled here, the energy surfaces reflect the geometry of the grain, with the hard directions along the grain vertices, and the easy anisotropy directions at the center of the grains faces (for the cuboids and octahedra), and at the center of the grain sides for the tetrahedral grains. This is in contrast to that of equivalent two-dimensional structures where the easy directions, and highest coercivities, are generally along the grain vertices [*Koltsov et al.*, 2000]. The main reason for this is the different remanence domain structures that can exist in thin film samples, such as the “S”-type structures, whose net magnetization lies along the grain diagonal [*Torres et al.*, 2001].

[27] The energy difference between the easy and hard anisotropy directions is strongly dependent on the grains shape, and the amount of flowering that can be accommodated within the grain. In all geometries, the highest magnetic energy density occurs for the smallest grains, but even here the magnetization is significantly nonuniform.

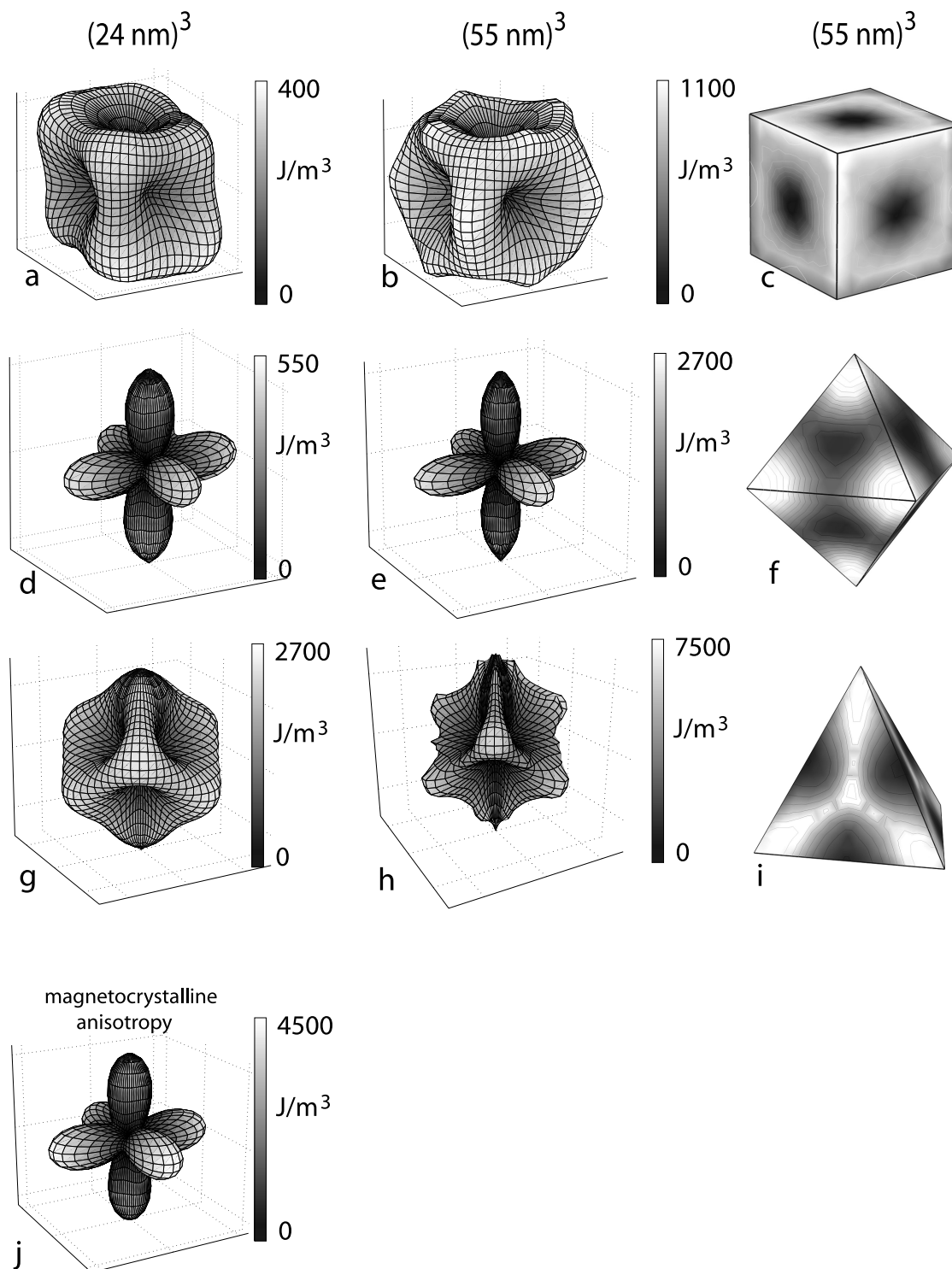


**Figure 4.** Configurational anisotropy energy surfaces for flower domain states in (a, b) cubes, (d, e) octahedral, and (g, h) tetrahedra. Figures 4a, 4d, and 4g show energy surfaces for grains of size  $(55 \text{ nm})^3$ , and Figures 4b, 4e, and 4h show energy surfaces for size  $(24 \text{ nm})^3$ . The grey scales indicate energy density in units of  $\text{J m}^{-3}$ . Figures 4c, 4f, and 4i show the configurational energy surfaces for the  $(55 \text{ nm})^3$  grains mapped onto their respective geometries, using the same grey scale. Figure 4j shows the magnetocrystalline anisotropy energy surface for magnetite, with the easy axis along  $\langle 111 \rangle$  and hard  $\langle 100 \rangle$ . See selected energy surfaces in color and in three dimensions in the related link in the HTML.

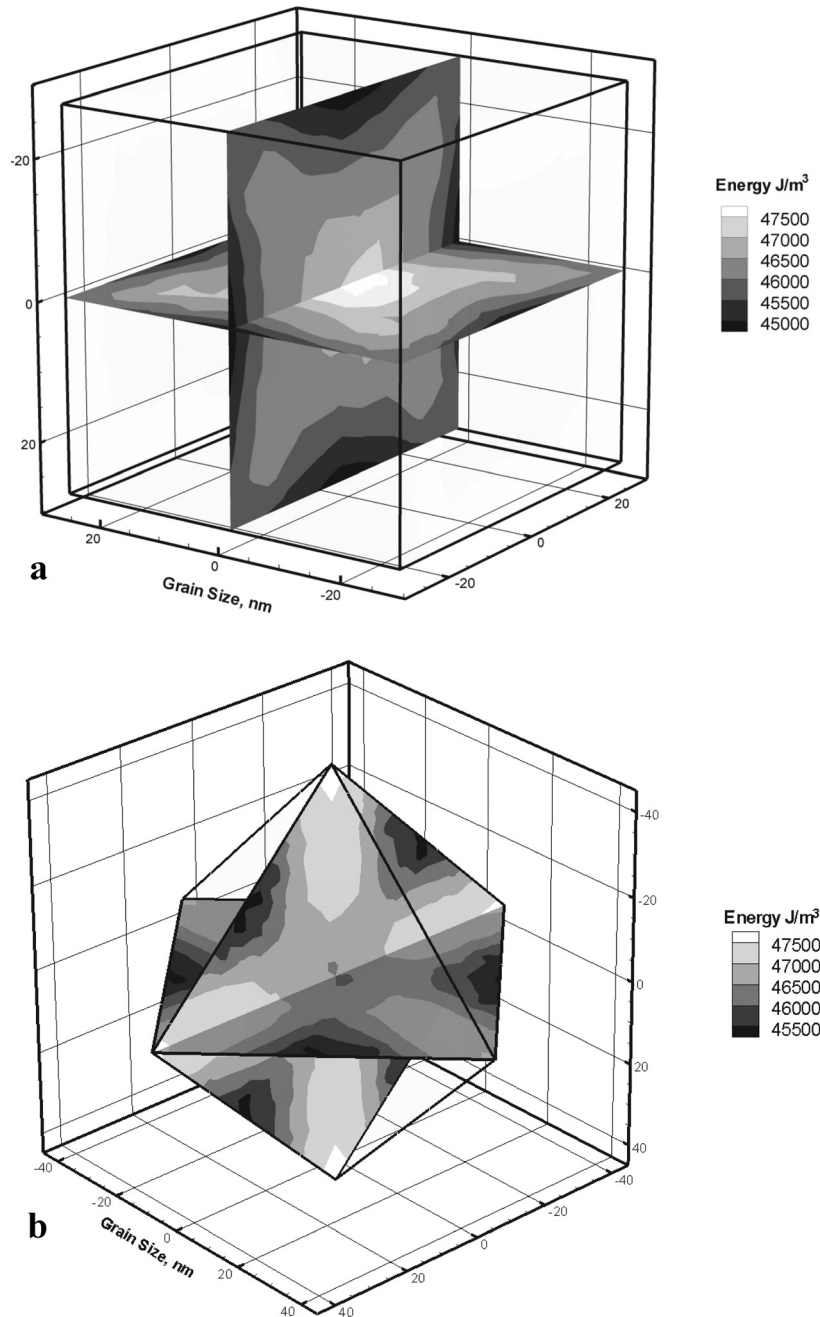


**Figure 5.** Polar plots of the configurational energy density for (a) cubes, (b) octahedral, and (c) tetrahedral. The radius gives the grain size in nm, and direction indicates the orientation of the flower domain state. For each geometry, two planes are selected which intersect at the centroid.

If we constrain the magnetization in the grains to be perfectly uniform, then the energy is shape independent and takes value of  $\sim 48,200 \text{ J m}^{-3}$  for all three geometries. This energy corresponds to the demagnetizing energy with an average internal demagnetizing field of  $\mu_0 M_S/3$ , and is independent of the magnetization direction. Therefore configurational anisotropy will not exist in uniformly magnetized grains. This maximum energy density decreases as soon as any nonuniformity (flowering) occurs in the magnetization. This can be best appreciated in a polar plot of the energy density, where the radius gives the grain size, and

direction (from the axis origin) gives the polar angles of constrained magnetization (Figure 5). As the grain size increases, the magnetization becomes less uniform, and the energy density decreases. At the same time, the energy difference between the hard and easy configurational anisotropy directions increases. In general, this will correspond to an increase in the coercivity with increasing grain size as seen in Figure 3b, provided the domain reversal path remains unchanged. A dip in the coercivity for the cubic and octahedral grains at  $(70 \text{ nm})^3$  indicates a change in reversal path for vortex domain states.

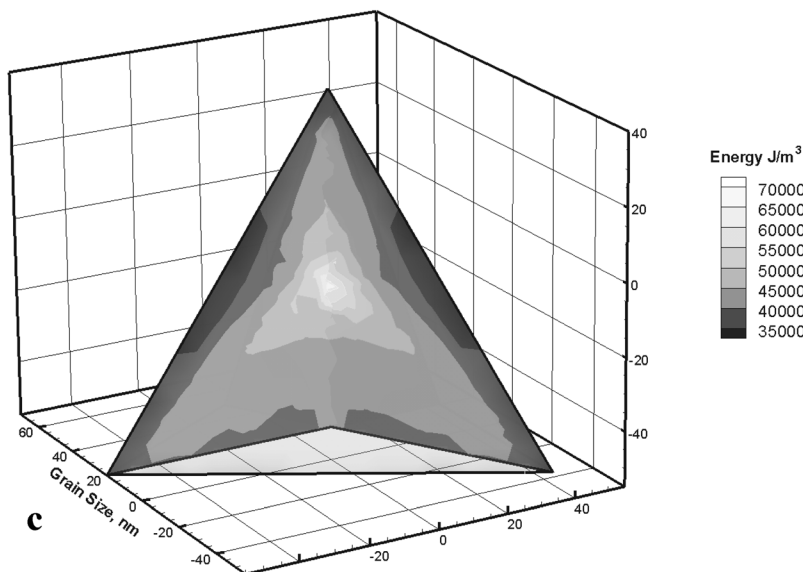


Figure 5. (continued)

[28] Also evident from Figure 5 is that the energy surface becomes more complex as the domain structure become less uniform. We would certainly expect this when vortex domain states interact with grain geometries, but it can be seen that even for flower states in the larger grains the symmetry of the energy surface deforms significantly. For the cubic grains, for example, the hard axis changes from the diagonal joining the grain vertices to that along the grain edge (compare Figures 4a and 4b).

#### 4.2. Comparison to the Magnetocrystalline Anisotropy and Elongated Grains

[29] The contribution of magnetite's cubic magnetocrystalline anisotropy to coercivity is easily calculated as  $H_k = \frac{4}{3}K_1/\mu_0M_S$  [Dunlop and Özdemir, 1997], and yields a value of  $\mu_0H_K = 34$  mT for the material parameters values we use. This result neglects the effect of thermal fluctuations, the magnitude of which scales as the inverse square of the grain volume, and which takes a value of  $\sim 10$  mT for a grain of size  $(50 \text{ nm})^3$ . Although thermal fluctuations are not included in the micromagnetic calculations, the analytical value of 34 mT is not achieved in hysteresis simulations, even for equidimensional grains in which the magnetization is constrained to be perfectly uniform. This is because, for coherent rotation of the magnetization, the energy barrier between easy magnetization directions rapidly decreases as the applied field approaches to within  $\sim 10$  mT of the analytic value of the critical (coercive) field. The minimum energy state for the magnetization oriented antiparallel to the applied field becomes very unstable. It is difficult to detect this as a valid equilibrium state compared with the much lower energy state that exists, where the magnetization has rotated toward the field direction.

[30] As a comparison between configurational and magnetocrystalline anisotropy, we have plotted on Figure 3b the coercivity of spherical grains of magnetite in which the cubic magnetocrystalline anisotropy is assumed. Spherical grains exhibit very little flowering since the internal demagnetizing field is almost uniform (and takes the value of  $\mu_0M_S/3$ ). The coercivity of 25 mT plotted in Figure 3b is the

value expected for magnetocrystalline anisotropy-controlled coercivity in numerical simulations. This remains constant until a vortex state is nucleated and noncoherent domain reversal occurs.

[31] The coercivities due to configurational anisotropy can be extremely large (Figure 3b), particularly when the grain's geometry allows significant reduction of the magnetization through flowering, as in the case of the tetrahedral grains. In these grains a maximum coercivity of 120 mT is attained at a grain size of  $(55 \text{ nm})^3$ . A peak in coercivity at this grain size also occurs for the cubic and octahedral grains. Beyond this grain size, the vortex domain state becomes the minimum energy state, and although the tetrahedral grain remains in a flower state, the large amount of flowering results in a lower energy barrier to domain reversal.

[32] As the grain size increases further for the tetrahedral grains, the reversal mechanism remains the same, but the coercivity decreases due to the reduction in the energy barrier as the amount of domain flowering increase. For the cubic and octahedral grains an additional peak in the coercivities is seen as the minimum energy domain state switches from one where the vortex core aligns along a grain diagonal to one where the core aligns normal to a grain face (Figures 1b, 1c, 1e, and 1f).

[33] The peak coercivity of 120 mT predicted for the tetrahedral grain would normally be associated only with highly acicular grains. Assuming that coercivity due shape anisotropy is given by  $\mu_0 H_C = (N_a - N_b)M_S$ , where  $N_a$  and  $N_b$  are the demagnetizing coefficients along the short and long axis, respectively, of a uniformly magnetized prolate ellipsoid [Nagata, 1961; Stacey and Banerjee, 1974], then for magnetite a 120 mT coercivity requires an axial ratio of  $\sim 0.57$ , or an elongation of 1:1.75. For an assemblage of randomly aligned grains, even higher axial ratios would be required to produce the same coercivities obtained from configurational anisotropy. This calculation neglects the additional effects of magnetocrystalline anisotropy, which will always be present in magnetite. However, for acicular

grains, shape anisotropy dominates as the elongation increases beyond 1:1.1.

[34] Compared to magnetite's magnetocrystalline anisotropy, the configurational anisotropy has a similar range of associated coercivities. Therefore in equidimensional grains the net coercivity will depend on the relative orientation of the crystalline and configurational anisotropy axis, with respect to both the field and each other, i.e., the two anisotropies may enhance each other or cancel each other out. This relationship between the anisotropy axes for the two different sources of anisotropy can be seen from examination of the energy surfaces in Figure 4. For cubic grains where the grain edges are aligned with the  $\langle 100 \rangle$  axis, then the magnetocrystalline easy axis coincides with the hard axis of the configurational anisotropies, a canceling effect. For octahedral grains with  $\{111\}$  surfaces, the opposite is true, and the magnetocrystalline and configurational anisotropies will coincide.

## 5. Conclusions

[35] The interaction between the domain state and grain geometry produces a magnetic anisotropy commonly termed configurational anisotropy, where the easy and hard axis of magnetization are related to the grain geometry, even for equidimensional grains. For SD and PSD grains of magnetite, we have shown that the magnitude of this effect can be similar, and sometimes far greater, than that of magnetocrystalline anisotropy. For tetrahedral shaped grains in particular, flower domain states can be accommodated with much lower magnetic energies than that of other shapes of equidimensional grains of a similar grain volume. This is achieved by a large degree of flowering, which produces a large energy barrier to coherent rotation.

[36] It is therefore possible to obtain large coercivities in magnetite without assuming highly acicular grain geometries and/or high levels of internal stress. Unlike acicular grains, the configurational anisotropy can have high degrees of symmetry, which can therefore produce high values of saturation remanence in randomly aligned arrays of particles, i.e.,  $M_{RS}/M_S > 0.5$ .

[37] **Acknowledgments.** We would like to thank Claire Carvallo and an anonymous reviewer for their helpful comments. This work was funded through NERC research grant NE/C510159/1 with additional funding from the Royal Society of London.

## References

- Cowburn, R. P., et al. (1999), Designing nanostructured magnetic materials by symmetry, *Europhys. Lett.*, *48*, 221–227.
- Dunlop, D. J., and O. Özdemir (1997), *Rock Magnetism: Fundamentals and Frontiers*, 573 pp., Cambridge Univ. Press, New York.
- Enkin, R. J., and W. Williams (1994), 3-dimensional micromagnetic analysis of stability in fine magnetic grains, *J. Geophys. Res.*, *99*, 611–618.
- Fredkin, D. R., and T. R. Koehler (1990), Hybrid method for computing demagnetizing fields, *IEEE Trans. Magn.*, *26*, 415–417.
- Heider, F., and W. Williams (1988), Note on temperature dependence of exchange constant in magnetite, *Geophys. Res. Lett.*, *15*, 184–187.
- Koltsov, D. K., et al. (2000), Micromagnetics of ferromagnetic equilateral triangular prisms, *J. Appl. Phys.*, *88*, 5315.
- Nagata, T. (1961), *Rock Magnetism*, 2nd ed., 350 pp., Maruzen, Tokyo.
- Pauthenet, R., and L. Bochirol (1951), Aimantation spontanée des ferrites, *J. Phys. Radium*, *12*, 249–251.
- Rave, W., et al. (1998), The magnetic states of small cubic magnetic particles with uniaxial anisotropy, *J. Magn. Magn. Mater.*, *190*, 332–348.
- Schrefl, T. (1999), Finite elements in numerical micromagnetics Part I: Granular hard magnets, *J. Magn. Magn. Mater.*, *207*, 45–65.
- Stacey, F. D., and S. K. Banerjee (1974), *The Physical Principles of Rock Magnetism*, 195 pp., Elsevier, New York.
- Torres, L., et al. (2001), Configurational anisotropy and thermally activated switching in magnetic nanosquares, *Physica B*, *306*, 216.
- Vavassori, P., et al. (2005), Magnetocrystalline and configurational anisotropies in Fe nanostructures, *J. Magn. Magn. Mater.*, *290*, 183–186.
- Williams, W., and D. J. Dunlop (1989), Three-dimensional micromagnetic modelling of ferromagnetic domain structure, *Nature*, *337*, 634–637.
- Williams, W., and T. M. Wright (1998), High resolution micromagnetic models of fine grains of magnetite, *J. Geophys. Res.*, *103*, 30,537–30,550.
- Witt, A., et al. (2005), Three-dimensional micromagnetic calculations for naturally shaped magnetite: Octahedra and magnetosomes, *Earth Planet. Sci. Lett.*, *233*, 311–324.
- Wright, T. M., et al. (1997), An improved algorithm for micromagnetics, *J. Geophys. Res.*, *102*, 12,085–12,094.

A. R. Muxworthy, Department of Earth Science and Engineering, Imperial College, South Kensington Campus, London, SW7 2AZ, UK.

G. A. Paterson, National Oceanography Centre, University of Southampton, European Way, Southampton, SO14 3ZH, UK.

W. Williams, School of Geosciences, University of Edinburgh, Kings Buildings, West Mains Road, Edinburgh, EH9 3JW, UK. (wyn.williams@ed.ac.uk)